STUDY OF THE HEAT TRANSFER PERFORMANCE OF A LOOP HEAT PIPE WITH ALUMINUM WICK

Bingyao LIN [1], Rongjian XIE[2*], Leren, TAO[1]

[1] School of Energy and Power Engineering, University of Shanghai for Science and Technology, Shanghai, PR China

[*2] Shanghai Institute of Technical Physics, Chinese Academy of Sciences, Shanghai, PR China

[*] Corresponding author; E-mail: linbingyao1017@163.com

This study used aluminum (Al) powder as a raw material to fabricate a wick for loop heat pipes (LHPs) by the powder metallurgy method and took advantage of the excellent corrosion resistance, low density and low cost of Al. The average pore diameter, porosity and permeability of the Al wicks were 9 μm, 47.65%, and 2.1×10^{-13} m^{-2}, respectively. Then, to verify the feasibility of the Al wick, it was installed into a LHP to test the heat transfer performance. The experimental results showed that the LHP could transport a heating load of 130 W with a thermal resistance of 0.04 KW-1 under horizontal condition. A steady-state LHP mathematical model was developed, and the numerical results were compared with the experimental data. The results show that the model data are consistent with the experimental data, which means that Al wicks are suitable for use in the case of a high heating load and light weight.

Key words*: heat transfer, loop heat pipe, wick, mathematical model*

1. Introduction

The rapid development of integrated circuit technology requires characteristics such as miniaturization and integration; thus, high-efficiency heat dissipation equipment is also required. LHPs are efficient two-phase heat transfer devices with porous wicks that pump the working fluid, and they are capable of transferring heat over long distances, maintaining thermal homogeneity, and operating in a microgravity environment. LHPs possess many advantages relative to conventional heat pipes, and they are capable of transferring heat for several meters, isolating mechanical vibration effectively and making the connection between the heat source and heat sink more flexible.

Porous wicks, as the critical component in LHPs, play a pivotal role in the operational process. The wick should possess an appropriate pore size distribution, porosity, thermal conductivity and permeability to produce a stable capillary force to circuit the working fluid and keep the LHP at a suitable operating temperature.

Due to the simple sintering process of copper powder, the most widely used materials for LHP wicks are copper, stainless steel, nickel, titanium, zirconia, etc. However, the density and thermal conductivity of copper are approximately 8.9 gcm-3 and 377 Wm–1K–1, respectively. The larger density and thermal conductivity limit the application of LHPs in many areas. Currently, the most widely used materials for processing wicks include copper, nickel, stainless steel, PTFE

(polytetrafluoroethylene), etc. Research shows that PTFE wicks have a good inhibitory effect on heat leakage[1-3] and relatively good heat transfer performance. However, these polymers usually have melting points lower than 327℃ and polymers have relatively larger contractions than metal materials in cryogenic areas. These characteristics certainly limit the application of LHPs in the fields of high temperature and low temperature. In addition, metallic wicks are also widely used. Guo[4] assembled an LHP with nickel wick to study the startup of a cryogenic loop heat pipe (CLHP) with redundancy and reliable and long-life operation. Experiments showed that its startup was affected by the inner diameter of the transport line and the distribution of working fluid in the system. Bai[5] fabricated a CLHP using a nickel wick to study the effect of the relative position of different components on the startup and operation of CLHPs. The position of the secondary loop line and CC is considered to have a strong influence on the startup of the CLHP. Zhou[6] produced a plate-type LHP using copper and nickel as wick materials to study the influence of multilayer wicks on the heat transfer performance of LHPs. Compared to the nickel foam, the LHP with multilayer copper foams with wick structures showed better performance with different heating loads because of the higher thermal conductivity and smaller pore size. Celata[7] described an experiment on an LHP with the evaporator in the shape of a flat disk with an active diameter of 50 mm and a thickness of 13 mm. The wicks were made of stainless steel, and water was used as the working fluid. The result showed that the thermal resistance of the LHP, which is the resistance from the evaporator external surface to the condenser external surface (refrigerant water sink), ranged from 3.33 to 50.7 KW–1. Wicks made of commonly used metal material have a higher density, which is of great significance for reducing the weight for aerospace missions; however, limited research has been conducted in this area.

Foamed Al has low density, high temperature resistance, strong fire resistance, corrosion resistance, sound insulation and noise reduction, and it shows good performance in the field of construction, aerospace, and machinery[8-13], which makes it an ideal material for porous wicks of LHPs. Few LHPs have included Al wicks, and the commonly used cold pressing sintering and hot pressing sintering methods commonly used in Al powder sintering are not suitable for the production of Al wicks because wicks produced by these methods have a very low porosity. Therefore, this paper attempts to use a loose sintering method to make Al wicks. In this study, an LHP equipped with an Al wick was fabricated by sintered Al particles. A test was conducted with a heating load of 80 W-130 W. To analyze the operating performance of Al porous wicks, a steady-state mathematical model of LHPs is developed.

2. Experimental setup

2.1. Al wick description

The density of Al is only 2.7 g cm-3, which is much lower than that of copper, nickel and stainless steel. This is very important for the application of LHPs in aircraft. Generally, the operating temperature of spacecraft and electronic equipment is between 200-350 K[14]. According to the calculation formula of the Dunbar Parameters[15, 16] (Eq. 1), the best working fluid in this temperature zone is ammonia. Related experiments show that when the channel heat pipe wall is made of Al or aluminum alloy, there is no performance degradation in the channel heat pipe. Therefore, Al and ammonia are compatible[17].

$$\mathrm{Du} = \frac{\lambda^{1.75}\sigma\rho_v}{\mu_v^{0.25}} \quad (1)$$

Where λ, σ, ρ_v, μ_v are the thermal conductivity, surface tension, vapor density and dynamic viscosity of the working fluid, respectively.

At present, the existing methods for producing foamed Al are not suitable for processing wicks due to the difficulty of controlling the foaming agent and the cost [18, 19]. This paper investigates the use of a loose sintering method to make wicks and does not add foaming agent or apply pressure to the powder, which greatly simplifies the process and reduces costs.

2.2. Wick manufacturing process

This study chose Al as the material to manufacture wicks. Fig. 1 shows the operational process of Al wick manufacturing. To select Al powder with a certain particle size, spherical Al powder was screened. Then, additive powder was added to the Al powder to assist the sintering process. Finally, the mixed powder was put into the mold for sintering. In terms of the sintering mechanism, a certain proportion of the additive powder can promote sintering but will also reduce the porosity.

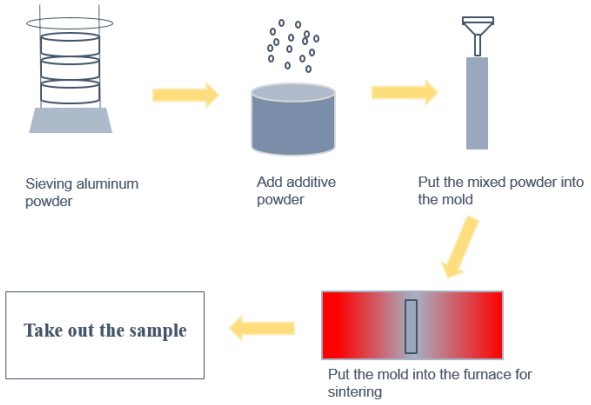

Fig. 1 Al wick manufacturing operation

2.3. Fabrication of LHP

The LHP studied in this paper is an ammonia-Al LHP equipped with an Al wick. The evaporator and the CC have an inner diameter of 20 mm. The wick consists of twelve vapor grooves and a liquid channel with diameters of 2 mm and 8 mm, respectively. The average pore size and porosity of the wick are 9 μm and 47%, respectively. All transport lines are made of Φ6×1.5 mm 6061Al pipes with lengths of 670 mm and 530 mm for the vapor and liquid lines. Fig. 2 shows a cross-sectional view of the evaporator and CC. The bayonet tube goes deep into the wick so that the returning liquid can infiltrate the wick faster, and a thin layer of secondary wick is observed on the inner wall of the CC so that the liquid in the CC can be supplemented to the evaporator as much as possible. In the experiment, the film heater was used as the simulated heat source. The film heater is directly attached to the evaporator casing, the heating element is controlled by DC power, and the output power range is 0~150 W.

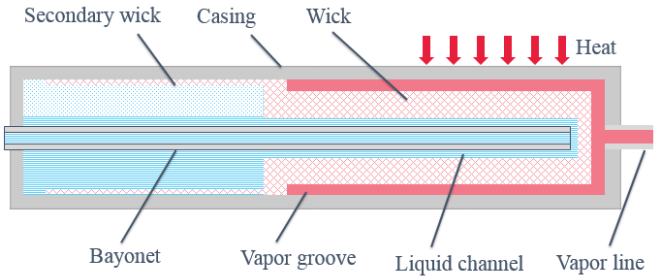

Fig. 2 Construction of the evaporator and CC

The temperature measurement system uses a T-type thermocouple, and the LHP has a total of 9 points. Fig. 3 shows the location of each measurement point. Two measuring points were allocated for each of the liquid lines, and one measuring point was allocated for each of the evaporators and the CC. Data were recorded every 20 seconds.

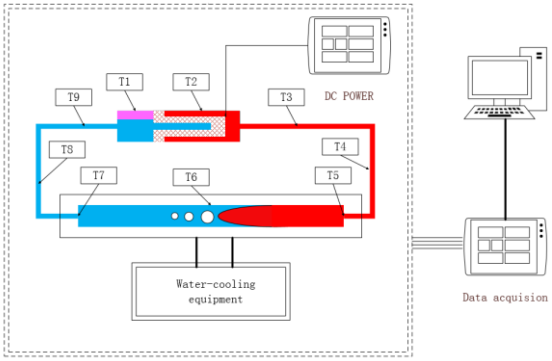

Fig. 3 figure of the LHP and the measurement system

After the experiment preparation is complete, the experiment on the heat transfer performance of the LHP begins. Fig. 4 shows the final test result of the LHP equip with an Al wick, and the performance parameters of the LHP are obtained. This study relies on these data to analyze the performance of the LHP and the consistency between the steady-state model data and the experimental data.

3. Experimental result

First, the water-cooling equipment was turned on to make the condenser temperature reach 295 K. After the temperature of all measuring points is stable, the DC power supply is turned on to heat the evaporator. After the heating load reached 80 W, the temperature of each measuring point showed a stable trend, and then the heating load was increased to 90 W; the rest of the heating load was deduced by analogy. The test data show that this LHP can run stably under a heating load of 130 W and the thermal resistance is approximately 0.04 KW-1. When the heating load reaches 140 W, the LHP will dry out; that is, the temperature of the evaporator increases dramatically while the temperature of the condenser drops linearly. Thermal resistance is calculated by Eq. (2):

$$\mathrm{R} = \frac{(T_{ev} - T_{cond})}{Q_{ap}} \tag{2}$$

It is worth noting that when the heating load is higher than 100 W, the temperature of the liquid line has a certain oscillation, with an amplitude of approximately 1 K and an oscillation period of approximately 4 minutes. It is believed that this oscillation is caused by the periodic movement of the vapor-liquid interface at the condenser outlet[20-22]. In this case, the liquid line has a large temperature oscillation amplitude and the evaporator and CC have a small amplitude.

The application temperature zone of ammonia is very wide, and the Dunbar parameter of ammonia is much higher than that of other working fluids in the same temperature zone. At present, copper wicks are the most commonly used in LHPs. Although both copper and Al are excellent conductors, copper is not compatible with ammonia. In addition, Al has relatively high tensile strength and is easy to process. The Al-ammonia LHP is of great significance for spatial applications of the LHP.

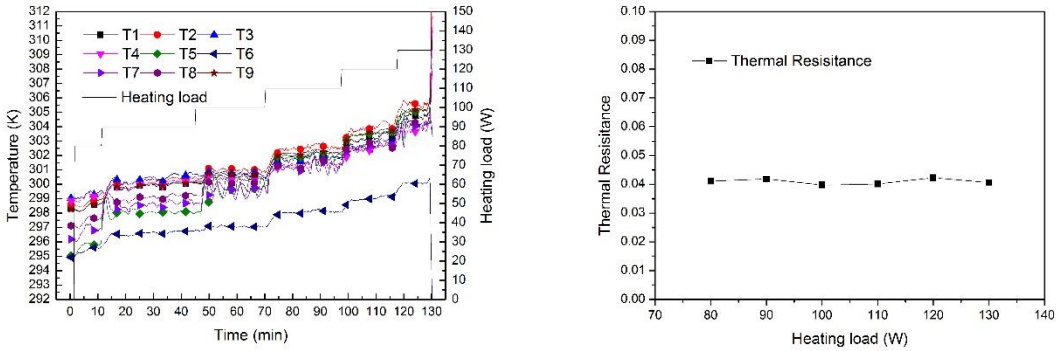

(a) (b)

Fig. 4 heat transfer performance under different heating load: (a) test result under different heating load. (b) thermal resistance under different heating load

4. Mathematical model

4.1. Assumption

To analyze the overall heat transfer performance of the Al-ammonia LHP, this section presents the establishment of the overall heat transfer model of the LHP. Traditional LHPs consist of an evaporator, CC, vapor line, liquid line and condenser. Fig. 2 shows the structure of the evaporator and CC and the distribution of the working fluid inside. The working fluid in the vapor line and liquid line are considered saturated vapor and saturated liquid, respectively. To facilitate the calculation and simplify the model, the following assumptions are made: (1) The vapor-liquid interface of the evaporator was assumed to be located in the outer surface of wick the whole time; (2) The condenser contains only two phase areas and subcooled areas; (3) The working fluid running into the CC from the liquid line is subcooled; (4) The local resistance in the transport line and condenser are neglected; and (5) The working fluid in the CC is saturated.

4.1.1 Transport line

Transport lines, including vapor lines and liquid lines, are generally composed of smooth metal pipes, and they usually connect the evaporator and the condenser. In the process of simulating the transport line, the local resistance and the thermal resistance of the pipe wall are generally ignored. When calculating the transport line, the outlet temperature T_{out} is first assumed. Because the temperature difference between the inlet and outlet of the transport line is quite small, the arithmetic mean temperature difference between the inlet and outlet of the transport line is used instead of the logarithmic average temperature difference. The vapor line calculation is taken as an example:

$$t_m = \frac{(T_{in} + T_{out})}{2} \tag{3}$$

where t_m is the characteristic temperature of the vapor line and T_{in} and T_{out} are the inlet and outlet temperatures of the vapor line, respectively. After obtaining the characteristic temperature, NIST is used to obtain the physical parameters of the working fluid. Then, the u_m, Re and Nu values of the working fluid can be calculated as follows:

$$u_m = \frac{m}{\pi r_i^2 \rho} \tag{4}$$

$$Re_f = \frac{u_m d_i}{\upsilon} \tag{5}$$

The value of Nu was calculated by the Dittus-Boelter equation:

$$Nu_f = 0.023 {Re_f}^{0.8} {Pr_f}^{0.4} \quad (t_w > t_m) \tag{6-a}$$

$$Nu_f = 0.023 {Re_f}^{0.8} {Pr_f}^{0.3} \quad (t_w < t_m) \tag{6-b}$$

$$h_f = \frac{Nu_f \lambda_f}{d_i} \tag{7}$$

$$h_1 = \frac{1}{h_f} + \frac{1}{2\pi\lambda_p} \ln\left(\frac{d_o}{d_i}\right) + \frac{1}{h_{p-amp}} \tag{8}$$

Heat exchange occurs between the vapor lines and the environment, which is hard to ignore. To calculate this part of the heat, we must first calculate the heat transfer coefficient between the pipeline and environment [23] :

$$h_{p-amb} = 1.32(\frac{T - T_{amb}}{d_o})^{0.25} \tag{9}$$

According to the energy conservation, taking the heat transfer coefficient as a fixed value, the following equations can be obtained:

$$\mathrm{Q}_{vl-amb} = \mathrm{m} c_p \Delta T \tag{10}$$

$$h_2 = \frac{\mathrm{Q}_{vl-amb}}{\pi r^2 L \Delta T} \tag{11}$$

Then, we can judge whether the calculated outlet temperature is reasonable. If $h_1 \approx h_2$, then temperature T_{out} is considered appropriate. Otherwise, reset T_{out}. Then, calculate the pressure drop ΔP in the transport line after obtaining T_{out}. The ΔP of the transport line is defined as follows:

$$\Delta \mathrm{P} = f \times \frac{1}{2} \times \rho_f \times {u_m}^2 \times \frac{4}{d_i} \times L_{vl} \tag{12}$$

$$f = \begin{cases} \dfrac{16}{Re} & Re < 2200 \\ \dfrac{0.079}{Re^{0.25}} & 2200 < Re < 10^5 \end{cases} \tag{13}$$

In this way, we can obtain the outlet temperature and pressure drop of the vapor line. The calculation process of liquid line is the same.

4.1.2 Evaporator

After the heating load Q_{ap} enters the evaporator, it is mainly divided into three parts:

$$Q_{ap} = Q_{latent} + Q_{sensible} + Q_{heatleak} \tag{14}$$

where Q_{latent} is the heat required for evaporation of the liquid working fluid in the wick (Eq. (15)); and $Q_{sensible}$ is the heat required to heat the liquid working fluid from the CC temperature to the evaporation temperature (Eq. (16)). Among them, latent heat is the main method of heat transfer.

$$Q_{latent} = mh_{fg} \tag{15}$$

$$Q_{sensible} = mc_p(T_{ev-sat} - T_{cc-sat}) \tag{16}$$

Mass flow (m) is a very important parameter, and it is calculated as follows:

$$m = \frac{Q_{ap} - Q_{sensible} - Q_{heatleak}}{h_{fg}} \tag{17}$$

The wick is a porous structure; therefore, the pressure drop inside the wick is calculated according to Darcy's law:

$$\Delta P_{wick} = \frac{m\mu_l \ln({}^{r_o}/_{r_i})}{2\pi\rho_l K L_{wi}} \tag{18}$$

A pressure drop will occur when the working fluid flows in the vapor grooves. This part of the pressure drop can be calculated as follows:

$$u_{vg} = \frac{m}{n\rho_v \pi r_{vg}^2} \tag{19}$$

$$L_{vg,eff} = \frac{L_{vg}}{2} \tag{20}$$

4.1.3 Condenser

The Lockhart-Martinelli separated flow model and Chato equation were used to calculate the two-phase region of the condenser [24]

According to the energy conservation, the heat released from the two-phase region of the condenser is equal to the heating load minus the heat leakage and vapor line heat leak:

$$Q_{tp} = Q_{ap} - Q_{heatleak} - Q_{vl-amb} \tag{21}$$

The heat transfer coefficient between the two-phase flow and inner wall of the condenser line can be calculated as follows:

$$h_{tp} = \frac{1}{\frac{1}{h_{tp-p}\pi d_i} + \frac{1}{2\pi\lambda_p}\ln(\frac{d_o}{d_i})} \tag{22}$$

The flow in the two-phase region is consistent with the Chato formula and Newton cooling formula:

$$h = 0.555\left(\frac{{\lambda_l}^3 \rho_l(\rho_l - \rho_v) g h'_{fg}}{\mu_l d_i (T_{sat} - T_{sink})}\right)^{0.25} \tag{23-a}$$

$$h'_{fg} = h_{fg} + \frac{3}{8}c_p(T_{sat} - T_{sink}) \tag{23-b}$$

$$L_{tp} = \frac{Q_{tp}}{h(T_{sat} - T_{sink})A_{cond}} \tag{23-c}$$

where A_{cond} is the cross-sectional area of the condenser and h is the heat transfer coefficient of condensation in the horizontal tube.

According to the Lockhart-Martinelli separated flow model, the pressure drop in the condenser is obtained as follows:

$$\frac{dF}{dz} = \frac{dF}{dx} * \frac{dx}{dz} \tag{24}$$

4.1.4 Compensation chamber

According to the mass conservation, the filling amount of the working fluid, M_{charge}, is equal to the sum of the working fluid mass in each component

$$M_{charge} = M_{eva} + M_{vl} + M_{ll} + M_{cond} + M_{cc} \tag{25}$$

The value of $\alpha_{l,CC}$ is an extremely important parameter for normal operation of the LHP. The liquid fraction of the CC can be calculated as follows [25]:

$$V_l = \frac{M_{cc} - \rho_v V_{cc}}{\rho_l - \rho_v} \tag{26-a}$$

$$V_v = \frac{\rho_l V_{cc} - M_{cc}}{\rho_l - \rho_v} \tag{26-b}$$

$$\alpha_{l,CC} = \frac{V_l}{V_{CC}} \tag{26-c}$$

If it is too small, then the rate of working fluid replenishment will be less than the rate of working fluid evaporation in the wick. Consequently, the vapor-liquid interface returns to the inner surface of the wick, and a dry out phenomenon occurs. If the value of $\alpha_{l,CC}$ is equal to 1, then the LHP works in a constant conductance area.

The capillary pressure should be larger than the total pressure drop of the circuit, which is an important basis to judge whether convergence occurs:

$$\frac{2\sigma}{r_p} \geq \Delta P_{eva} + \Delta P_{vg} + \Delta P_{vl} + \Delta P_{ll} + \Delta P_{cond} + \Delta P_{gravity} \tag{27}$$

According to the principle of energy conservation, subcooled liquid returned to the CC should neutralize the heat leakage and heat exchange between the CC and the environment:

$$Q_{heatleak} + Q_{cc-amb} = Q_{sub-cc-in} \tag{28}$$

The energy equation of the CC is the most important factor for judging whether the calculation converges. The main method of calculating heat leakage is to simplify the heat leakage into the form of cylindrical radial heat conduction or to calculate the heat transfer coefficient experimentally. The former hypothesis is used in this paper (Eq. 29).

$$Q_{heatleak} = G_{HL}(T_{ev} - T_{CC}) \tag{29-a}$$

$$G_{HL} = mc_{p,CC} \frac{\left(\frac{r_i}{r_o}\right)^{\eta}}{1 - \left(\frac{r_i}{r_o}\right)^{\eta}} \tag{29-b}$$

$$\eta = \frac{mc_{p,CC}}{2\pi\lambda_{wick,eff} L_{wick}} \tag{29-c}$$

4.2. Solution algorithm

The solution flow chart of the above model for the LHP is shown in Fig. 5. The initial value of the evaporation temperature should not be set too small; otherwise, the pressure drop in the circuit will be too large, and Eq. (27) cannot be satisfied.

The results of Eq. (28) are used to judge whether the results meet the requirements of energy conservation, which is a necessary condition for the steady-state model. If energy conservation is not satisfied, then the evaporation temperature continues to iterate at + 0.01 K until the condition is met or the calculation of the critical temperature fails. The physical meaning of energy conservation of the CC is that the subcooled degree of the working fluid flowing back from the liquid line compensates for the heat leakage and the heat exchange between the CC and the environment. The heat transfer between the CC and the environment is natural convection in ground-based applications.

Since $Q_{sensible}$和$Q_{heatleak}$ are unknown at the beginning of the calculation, Q_{ap} is used to calculate m

$$m = \frac{Q_{ap}}{h_{fg}} \tag{30}$$

Then $Q_{sensible}$和$Q_{heatleak}$ can be obtained, and m can be modified by Eq. (17).

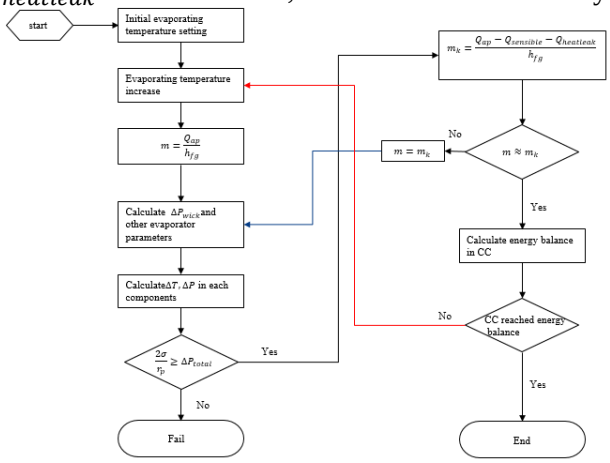

Fig. 5 Mathematical model calculate flow chart

4.3. Mathematical model verification

To verify the feasibility of this mathematical model, the calculated results of the model are compared with the experimental results of the LHP in this work (Fig. 6).

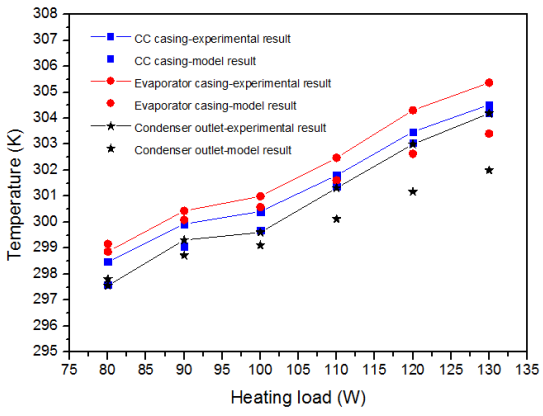

Fig. 6 Comparison of the model calculation results and experimental results

As shown in Fig. 6, the discrepancy between the model results and the experimental results is approximately 3 K, and the trend of temperature change with heating load is similar to the experimental results, which proves that the model is reasonable and effective. However, there are still some differences between the model calculation results and the experimental results, and these differences increase with increasing heating load.

(1) In the model, the vapor-liquid interface is assumed to be on the surface of the wick, while in reality, it begins to retreat to the evaporator core when the heating load reaches the critical heating load. The wick area above the vapor-liquid interface is filled with saturated vapor working fluid.

Moreover, the effective thermal conductivity of the wick will also change at this time, resulting in a change in the form and value of heat leakage. This change could be increasingly obvious with increasing heating load. In addition, when the vapor-liquid interface retreats to the inside of the evaporator, the bubble will also hinder the flow of the working fluid.

(2) In the cryogenic experiment, the heat exchange between the condenser and the environment is very small and the lowest temperature in the condenser is at the outlet of the condenser; however, in the normal temperature test, the outlet temperature of the condenser is not the lowest. Even with polyamide thermal conductive sheets, a certain level of contact thermal resistance is observed between the condenser and the water-cooled plate. On the other hand, the subcooled area in the condenser behind the two-phase area is actually under the influence of the environment and heat sink. The calculation of this part remains to be studied. In addition, the pressure drop calculated by the Lockhart-Martinelli separated flow model is relatively larger than reality, which is also one of the reasons for the difference between the calculated value and the experimental value.

(3) The model assumes that the working fluid in the CC is saturated. In actual operation, the vapor working fluid in the CC mainly comes from the evaporation of the inner surface of the wick caused by the guide heat of the diameter of the free wick; therefore, the temperature is higher than the saturation temperature of the CC. In addition, the heat transfer through the casing between the evaporator and the CC is also a factor that causes the difference.

5. Conclusion

This paper chose Al powder as the material to prepare the LHP evaporator. The evaporator was assembled into the LHP, and a heat transfer performance test was carried out. Then, a steady-state mathematical model of the LHP was established, and the experimental data were compared with the model calculation results. The main conclusions can be summarized as follows.

1. In this study, Al powder is used as the material of the porous wick of the LHP, and the wick is manufactured by powder metallurgy, thus verifying the feasibility of the Al-ammonia LHP.

2. For the lightweight trend of LHP, the heat transfer performance of the Al-ammonia LHP was tested. The results show that the Al-ammonia LHP could transfer a heating load of 130 W and the thermal resistance was approximately 0.04 KW-1. During the experiment, the LHP can reach the heat balance quickly, and the temperature has no obvious fluctuation, which verifies the feasibility of the Al wick.

3. Based on energy conservation, a steady-state mathematical model of the LHP is established, and the calculated results are compared with the experimental data. The results show that the calculated results are consistent with the experimental data.

Nomenclature

A	area of cross section (m2)	Greek symbols	
c_p	specific heat capacity(Jkg-1mol-1)	ε	porosity
d	diameter (m)	μ	dynamic viscosity(Pa×s)
Du	Dunbar parameter (W1.75m-2.75)	ρ	Density(kgm-3)
h	heat transfer coefficient (Wm-2K-1)	α	volume fraction
h_{fg}	latent heat of vaporization (Jkg–1)	υ	kinematic viscosity((m2s–1)
K	permeability	Δ	change
L	length (m)	λ	thermal conductivity (Wm–1K–1)
M	mass (kg)	Subscripts	
m	mass flow (kgs–1)	cc	compensation chamber
Pr	Prandtl number	cond	condenser
P	pressure (Pa)	eff	effective
Q	heat quantity (W)	ev	evaporator
Re	Reynolds number	l	liquid
R	thermal resistance (m2K-1W–1)	ll	liquid line
r	radius (m)	p	pipe
T	temperature (K)	sat	saturated condition
u	velocity (ms–1)	tp	two phase
x	dryness	vg	vapor groove
		vl	vapor line
		v	vapor

References

[1] Tingting, H., *et al.*, Heat transfer performance of polytetrafluoroethylene oscillating heat pipe with water, ethanol, and acetone as working fluids, *International Journal of Heat and Mass Transfer*, *131*. (2018), pp. 109-120, DOI No. 10.1016/j.ijheatmasstransfer.2018.08.133

[2] Laura Fourgeaud, R.M., Vincent Dupont, Christophe Figus, *Experimental investigations of a Multi-Source Loop Heat Pipe for electronics cooling*, *Joint 19th IHPC (International Heat Pipe Conference) and the 13th IHPS (International Heat Pipe Symposium)*. 2018: Pisa.

[3] Mitomi, M.,H. Nagano, Long-distance loop heat pipe for effective utilization of energy, *International Journal of Heat and Mass Transfer*, *77*. (2014), pp. 777-784, DOI No. https://doi.org/10.1016/j.ijheatmasstransfer.2014.06.001

[4] Guo, Y., *et al.*, Experimental study on the supercritical startup of cryogenic loop heat pipes with redundancy design, *Energy Conversion and Management*, *118*. (2016), pp. 353-363, DOI No. https://doi.org/10.1016/j.enconman.2016.04.022

[5] Bai, L., *et al.*, Effect of component layout on the operation of a miniature cryogenic loop heat pipe, *International Journal of Heat and Mass Transfer*, *60*. (2013), pp. 61-68, DOI No. https://doi.org/10.1016/j.ijheatmasstransfer.2013.01.011

[6] Zhou, W., *et al.*, Development and tests of loop heat pipe with multi-layer metal foams as wick structure, *Applied Thermal Engineering*, *94*. (2016), pp. 324-330, DOI No. https://doi.org/10.1016/j.applthermaleng.2015.10.085

[7] Celata, G.P., *et al.*, Experimental tests of a stainless steel loop heat pipe with flat evaporator, *Experimental Thermal and Fluid Science*, *34*. (2010), pp. 866-878, DOI No. 10.1016/j.expthermflusci.2010.02.001

[8] Figueroa, I.A., *et al.*, Mechanical behavior of heat-treated Al-Cu-Mg open-cell foams, *Materials Letters*, *284*. (2021), p. 129021, DOI No. https://doi.org/10.1016/j.matlet.2020.129021
[9] Liang, L., *et al.*, Radial Basis Function Neural Network for prediction of medium-frequency sound absorption coefficient of composite structure open-cell aluminum foam, *Applied Acoustics*, *170*. (2020), p. 107505, DOI No. https://doi.org/10.1016/j.apacoust.2020.107505
[10] Tang, E., *et al.*, Simulation of CFRP/aluminum foam sandwich structure under high velocity impact, *Journal of Materials Research and Technology*, *9*. (2020), 4, pp. 7273-7287, DOI No. https://doi.org/10.1016/j.jmrt.2020.04.093
[11] Garai, F., *et al.*, Development of tubes filled with aluminium foams for lightweight vehicle manufacturing, *Materials Science and Engineering: A*, *790*. (2020), p. 139743, DOI No. https://doi.org/10.1016/j.msea.2020.139743
[12] Wan, T., *et al.*, Fabrication, properties, and applications of open-cell aluminum foams: A review, *Journal of Materials Science & Technology*, *62*. (2021), pp. 11-24, DOI No. https://doi.org/10.1016/j.jmst.2020.05.039
[13] Santhosh, S., *et al.*, Fabrication and analysis of aluminium foam with glass fiber based on PMC for helmet applications, *Materials Today: Proceedings*. (2020), DOI No. https://doi.org/10.1016/j.matpr.2020.06.461
[14] Muenzel, W., Compatibility tests of various heat pipe working fluids and structural materials at different temperatures. (1978), DOI No. 10.2514/6.1978-398
[15] Bai, L., *et al.*, Development of cryogenic loop heat pipes: A review and comparative analysis, *Applied Thermal Engineering*, *89*. (2015), pp. 180-191, DOI No. https://doi.org/10.1016/j.applthermaleng.2015.06.010
[16] Su, Q., *et al.*, A review of loop heat pipes for aircraft anti-icing applications, *Applied Thermal Engineering*, *130*. (2018), pp. 528-540, DOI No. https://doi.org/10.1016/j.applthermaleng.2017.11.030
[17] Eninger, J.E., *et al.*, Heat Pipe Materials Compatibility, 'Report, NASA, America, 1976.
[18] Zhenhai, Y., *et al.*, Review and prospect of foamed aluminum in China and other countries, *Light Metals*. (2004), 6, pp. 3-6
[19] Yuyuan, Z., Sintering and Dissolution Process: A Novel Method for Manufacturing Aluminium Foams, *World Sci-Tech R & D*, *25*. (2003), 1, pp. 66-71
[20] Wang, N., *et al.*, Transient behaviors of loop heat pipes for alpha magnetic spectrometer cryocoolers, *Applied Thermal Engineering*, *68*. (2014), 1, pp. 1-9, DOI No. https://doi.org/10.1016/j.applthermaleng.2014.03.047
[21] Chen, Y., *et al.*, Steady-state and transient performance of a miniature loop heat pipe, *International Journal of Thermal Sciences*, *45*. (2006), 11, pp. 1084-1090, DOI No. https://doi.org/10.1016/j.ijthermalsci.2006.02.003
[22] Lu, X.-y., *et al.*, Thermal analysis of loop heat pipe used for high-power LED, *Thermochimica Acta*, *493*. (2009), 1, pp. 25-29, DOI No. https://doi.org/10.1016/j.tca.2009.03.016
[23] Bai, L., *et al.*, Mathematical modeling of steady-state operation of a loop heat pipe, *Applied Thermal Engineering*, *29*. (2009), 13, pp. 2643-2654, DOI No. https://doi.org/10.1016/j.applthermaleng.2008.12.040
[24] Zhongqi, L., *Two Phase Flow and Boiling Heat Transfer*. Tsinghua University Press, 2002.
[25] Vlassov, V.V.,R.R. Riehl, Mathematical model of a loop heat pipe with cylindrical evaporator and integrated reservoir, *Applied Thermal Engineering*, *28*. (2008), 8, pp. 942-954, DOI No. https://doi.org/10.1016/j.applthermaleng.2007.07.016

- Paper submitted: 04 September 2020
- Paper revised 04 August 2021
- Paper accepted: 07 August 2021